JOURNAL OF GEOPHYSICAL RESEARCH, VOL. 113, C08037, doi:10.1029/2007JC004407, 2008

Effects of atmospheric particles from Southern California on the optical properties of seawater

Malgorzata Stramska,[1] Dariusz Stramski,[2] Marta Cichocka,[2] Agnieszka Cieplak,[2]
and Sławomir B. Woźniak[3]

Received 19 June 2007; revised 8 April 2008; accepted 16 April 2008; published 22 August 2008.

[1] The role of particles deposited from the atmosphere to the ocean is poorly understood in ocean optics. We examined the light absorption and scattering properties of atmospheric particulate matter, which was collected by dry deposition near the Pacific coastline in La Jolla, Southern California, and then suspended in particle-free seawater for subsequent laboratory measurements. Within these suspensions, we measured the spectral absorption and beam attenuation coefficients, particle size distribution, and particle mass concentration of atmospheric particles. We also determined the 4-week average aerosol deposition rates at the experimental site over a period of 9 months. The mass-specific particle absorption $a_p^*(\lambda)$ and scattering $b_p^*(\lambda)$ coefficients showed considerable variability among the samples because of the variations in particle size distribution and composition. For example, $a_p^*(440)$ was on average 0.042 m^2 g^{-1} but exhibited over fivefold range among the samples. At near-infrared wavelengths (750–800 nm), the magnitude of a_p^* was significant (>0.02 m^2 g^{-1} for a number of samples) and is likely attributable to the presence of black carbon. The $b_p^*(\lambda)$ values were virtually wavelength-independent because of the significant presence of relatively large particles (>10 μm) in our samples. The magnitude of $b_p^*(\lambda)$ varied within a 3.5-fold range, with an average value of $\sim$0.27 m^2 g^{-1}. Our determinations of absorption and scattering by atmospheric particles coupled with radiative transfer simulations suggest that aerosol deposition may have sizable effect on ocean optical properties, including remote sensing reflectance under certain scenarios of deposition events, residence time of deposited particles within the water column, and particle properties.

Citation: Stramska, M., D. Stramski, M. Cichocka, A. Cieplak, and S. B. Woźniak (2008), Effects of atmospheric particles from Southern California on the optical properties of seawater, *J. Geophys. Res.*, *113*, C08037, doi:10.1029/2007JC004407.

1. Introduction

[2] Natural seawater is a complex optical medium consisting of a great variety of particle types with different sizes, shapes, refractive indices, and therefore different optical properties. As a result, simple optical or bio-optical parameterizations of seawater in terms of a few bulk particle categories or particle characteristics (such as total particulate matter, phytoplankton, and nonphytoplankton particle categories or total chlorophyll *a* and total particle mass concentrations) do not perform sufficiently well in all oceanic regions, particularly in complex coastal environments. It has long been recognized that the same total chlorophyll *a* concentration or particle mass concentration in water can produce significantly different absorption and scattering of light in the ocean. For example, significant variability in chlorophyll *a*-specific absorption and scattering coefficients has been shown for marine phytoplankton, both among the species and for a single species undergoing acclimation to varying growth conditions [e.g., *Bricaud et al.*, 1988; *Stramski and Morel*, 1990]. Similarly, significant variability in the spectral mass-specific particle absorption, $a_p^*(\lambda)$, and scattering, $b_p^*(\lambda)$, coefficients was demonstrated for mineral-rich particulate assemblages suspended in seawater [*Bowers et al.*, 1996; *Babin et al.*, 2003; *Babin and Stramski*, 2004; *Bowers and Binding*, 2006; *Stramski et al.*, 2007].

[3] The optical variability produced by variations in the detailed composition of particulate assemblages represents a major challenge that needs to be addressed through studies of various particle types such as different plankton groups and species, different types of other biogenic particles, different mineral-dominated particulate assemblages, and mixed organic-inorganic particle types and assemblages. This research strategy, which can be referred to as the reductionist approach, ultimately aims at developing optical models and parameterizations of natural waters in terms of a certain manageable number of particle functional groups

---

[1] Center for Hydro-Optics and Remote Sensing, San Diego State University, San Diego, California, USA.

[2] Marine Physical Laboratory, Scripps Institution of Oceanography, University of California at San Diego, La Jolla, California, USA.

[3] Institute of Oceanology, Polish Academy of Sciences, Sopot, Poland.

0148-0227/08/2007JC004407$09.00

that are optically and biogeochemically significant [e.g., *Stramski et al.*, 2001, 2004a, 2007].

[4] This study is focused on the optical properties of atmospheric particles upon their dry deposition and suspension in seawater. The optical properties of aerosols have been of great interest to atmospheric research in the past decades, primarily because of the role of aerosols in the Earth's radiative budget and climate forcing assessments [e.g., *Ramanathan et al.*, 2001; *Kaufman et al.*, 2002]. Long-range atmospheric transport of aerosols originating from natural and anthropogenic sources and their deposition in the ocean are relatively well documented [e.g., *Duce et al.*, 1980; *Prospero*, 1996; *Husar et al.*, 1997; *Jaffe et al.*, 1999]. The importance of connections between the deposition of aerosols and marine biogeochemical processes and sedimentary records has long been recognized [e.g., *Charlson et al.*, 1987; *Duce et al.*, 1991; *Martin et al.*, 1994; *Rea*, 1994; *Shinn et al.*, 2000]. There has also been significant interest in aerosol optical properties for the atmospheric correction of satellite ocean color imagery [e.g., *Gordon*, 1997; *Antoine and Morel*, 1999; *Nobileau and Antoine*, 2005]. However, the effects of particles deposited from atmosphere to the ocean on light absorption and scattering properties of seawater remain unquantified and poorly understood. Nevertheless, it has been recently suggested that the events of atmospheric dust deposition may have sizable effect on the bulk inherent optical properties (IOPs) of seawater and ocean color [*Twardowski et al.*, 2001; *Claustre et al.*, 2002; *Stramski et al.*, 2004b].

[5] Direct determinations of the optical properties of marine particles that originate from atmospheric deposition would be very difficult, if not impossible, to make in natural seawater samples because of the intervening effects of many types of other marine particles. In this study we report on laboratory measurements of atmospheric particles suspended in particle-free seawater. The particles were collected at a near-shore location at the Scripps Institution of Oceanography in La Jolla, California, over a period of 9 months from May 2005 through February 2006. In the Southern California coastal region, typically there are extended periods with little or no precipitation throughout much of the year when the dry deposition of atmospheric particles occurs. This study is focused on particles collected by dry deposition. We note that dry-deposited assemblages of atmospheric particles will typically exhibit different characteristics compared with wet-deposited assemblages, but the characterization of wet deposition is beyond the scope of this study.

[6] Our sampling site provided an opportunity to collect a fairly complex mix of atmospheric particles including mineral-rich dust originating from arid areas of southern California [*Hu and Liu*, 2003] and anthropogenic aerosols that contain a variety of compounds [*Li et al.*, 1997; *Hughes et al.*, 1999; *Christoforou et al.*, 2000; *Novakov et al.*, 2003]. Among the various aerosol species are mineral particles, organic particles, highly reflective sulfates, and strongly absorbing soot particles, generally referred to as black carbon (BC) that originates from fossil fuel combustion and biomass burning. We measured the spectral absorption and scattering coefficients of particles, particle size distribution, and particle mass concentration of aerosol samples suspended in seawater. We also determined the 4-week average values of aerosol deposition rates throughout the 9-month period at the experimental site. The mass-specific optical coefficients of atmospheric particles determined from our laboratory measurements and the estimated aerosol dry deposition fluxes in the Southern California coastal region were used to assess the influences of atmospheric particles on ocean remote sensing reflectance through numerical simulations with radiative transfer model. Thus the specific objectives of this study are to optically characterize the assemblages of atmospheric particles obtained by dry deposition in a particular coastal location and to use these data in preliminary assessments of potential influence of such assemblages on ocean reflectance.

2. Data and Methods

2.1. Collection of Samples

[7] Samples of atmospheric particulate matter were collected by dry deposition on the roof of the Scripps Institute of Oceanography NTV Building about 8 m above the ground level. The Pacific coastline is located less than 0.5 km to the west from the sampling site, and is situated within the San Diego metropolitan area. The samples were collected in clean plastic cylindrical buckets with an exposure area of 0.07 m^2. The buckets were cleaned with deionized filtered (0.2 μm) water in the laboratory before the sample collection. These buckets were placed on the roof inside larger containers to decrease the effects of air turbulence, for example, to prevent collection of particulate material previously deposited on the roof. This sampling setup favors collection of particles which are falling out vertically in the air, which probably results in an underestimation of the aerosol deposition rate. The experiment was carried out for 9 months from 18 May 2005 through 17 February 2006.

[8] The sampling strategy was as follows. First, two buckets were placed on the roof. After two weeks, two more buckets were added. After two more weeks, the first pair of buckets was taken for laboratory analysis and was replaced by a new pair of buckets, while the second pair of buckets on the roof continued to be exposed for the next two weeks. This means that each pair of buckets was normally recovered after a 4-week exposure period, and the two pairs of buckets had a 2-week overlap in the exposure period. Occasionally the exposure period was different (once 7 days, twice 14 days, and once 21 days) because the collection of samples was terminated earlier because of the anticipation of rain. The main rationale behind our general procedure to collect samples by dry deposition over 4-week periods was to collect enough particles necessary to prepare sufficiently concentrated particle suspensions in seawater required for our optical measurements. In addition, the samples are representative of particles deposited during dry weather conditions that typically occur in the Southern California over extended periods during much of the year. Significant rain events were rare during the experiment. The most significant rain event occurred on 16 through 19 October 2005. The sample collected during a period including that event is not used for optical characterization of particles but the aerosol deposition flux was still estimated for that sample. On several occasions during the experiment, minor rain events occurred

during a period of sample collection but in these cases only trace amounts of precipitated water was found in the buckets. This rainwater was evaporated in the laboratory before the preparation of particle suspension in seawater for subsequent measurements. Overall 18 samples were collected mostly as a result of dry deposition during the period of experiment and these samples are used for the characterization of optical properties of atmospheric particulate matter suspended in seawater.

[9] The meteorological data used in this study were recorded at the Montgomery Field in San Diego and obtained from California Climate Data Archive (www.calclim.dri.edu). These data include daily averages of wind speed, wind gusts, wind direction, and relative air humidity, as well as daily accumulated precipitation.

2.2. Laboratory Measurements

[10] Seawater from the pier of the Scripps Institution of Oceanography filtered through the 0.2 μm Nalgene sterile filters was used to prepare the samples of particle suspension. After collection of aerosol samples, the buckets were brought to the laboratory and 100 mL of filtered seawater were added (in 2–3 steps) to each bucket to produce a suspension of particles. Special efforts and care were devoted to wash the particles off the bucket surface and to achieve the best possible efficiency of resuspension of particles. Although the possibility of selective retrieval of particles into suspension cannot be excluded (for example, because of stronger electrostatic adhesion of very small particles to the bucket surface compared with larger particles), this problem is expected to be very small or insignificant. The visual inspection of the buckets indicated a very high percentage of recovery of particles into suspension. Whereas a large amount of bulk particulate matter was clearly visible in the bucket before resuspension, the particles left over in the buckets were unnoticeable after the completion of the preparation of particle suspension.

[11] The resulting particle suspension was transferred to precleaned glass bottles. The volume of seawater that was used to produce particle suspensions ensured appropriate concentration of particles for optical measurements. A portion of the sample from one bucket ($\sim$20 mL) was analyzed for the spectral particulate absorption coefficient, $a_p(\lambda)$, the spectral particulate beam attenuation coefficient, $c_p(\lambda)$, and particle size distribution, PSD. The remaining portion of the sample ($\sim$80 mL) and a sample from the second bucket ($\sim$100 mL) were filtered onto preweighted 0.2 μm polycarbonate membrane filters (Nuclepore, Whatman) for the determination of dry mass concentration of suspended particulate matter, SPM.

[12] Two or three subsamples from each bucket were filtered onto separate filters to determine SPM. The final estimate of SPM for each bucket was calculated from the determinations made on these two or three subsamples. After filtration, the filters were dried at room temperature in a dessicator at a relative humidity of 30–40% for 2–3 days before measuring the weight of particles with a Mettler-Toledo MT5 microbalance (resolution 0.001 mg). Each filter was weighed three times and the reproducibility of these measurements was better than 5%. The separate estimates of SPM for the two buckets differed on average by $\sim$30%. These differences can result from the inherent uncertainties of the SPM methodology, differences in the efficiency of aerosol deposition between both buckets, and some variation in the efficiency of resuspending particles in the buckets. Therefore the average SPM obtained from the two buckets was used as a final result. The determinations of total mass of particles collected in the bucket, the bucket area, and the duration of the bucket exposure were used to estimate the average aerosol deposition flux, Φ_d, for each exposure period during the experiment.

[13] For optical measurements we used methods described earlier [*Babin and Stramski*, 2002, 2004; *Stramski et al.*, 2004b, 2007]. The spectral absorption coefficient of particles, $a_p(\lambda)$, was measured with a dual-beam spectrophotometer (Lambda 18, Perkin Elmer) equipped with a 15-cm Spectralon integrating sphere (RSA-PE-18, Labsphere). The optical density, OD, was measured in the spectral range from 300 to 800 nm with a 1-nm interval using a 2-nm slit and a scan speed of 120 nm/min. The determinations of $a_p(\lambda)$ were made from a measurement of particle-free reference (i.e., strictly speaking the 0.2 μm filtered seawater) followed by a measurement of sample of particle suspension. These measurements were made in a 1-cm quartz cuvette placed in a special holder inside the integrating sphere. This geometry ensures that the absorption measurement of particles in suspension is subject to a small scattering error [*Babin and Stramski*, 2002]. First, the baseline spectrum of OD was measured twice on filtered seawater. Next, two replicate scans of OD were made on particles suspended in filtered seawater. One issue that needed special attention was that larger particles tended to settle in the cuvette during the spectral scan. Therefore the measurements on particle suspensions were made within 200 nm portions of the spectrum and the sample was mixed between scanning these portions. This procedure was repeated two times. The replicate scans were then merged and averaged to provide the final sample spectrum of OD. The average baseline was subtracted from the average sample spectrum to yield the final spectrum due to particles. The spectral absorption coefficient of particles, $a_p(\lambda)$ in m^{-1}, was calculated by multiplying the baseline-corrected OD values of the sample by ln(10) and dividing by the path length (=0.01 m).

[14] With our setup for absorption measurements one may observe a small artifact, i.e., a relatively small negative offset in the measured OD values when true absorption of particles is null or very weak, which usually occurs in the near-infrared (near-IR) spectral region ($\sim$700–850 nm) [*Babin and Stramski*, 2002, 2004]. This offset has been attributed to a difference in the light reflected by cuvette walls and escaping from the integrating sphere when the measurement of the scattering sample is compared to the baseline measurement of particle-free reference. A simple way of correcting for this artifact would be to shift the baseline-corrected spectrum by a value corresponding to the offset in the near IR, so that the resultant absorption values at these wavelengths are zero. This type of correction is often referred to as a null-point correction. The problem with such correction is that it will lead to an underestimate of true absorption for particle assemblages that exhibit sizable absorption in the near IR [e.g., *Tassan and Ferrari*, 2003; *Babin and Stramski*, 2004; *Bowers and Binding*, 2006]. To address this problem, *Stramski et al.* [2007] used

a different correction approach which takes advantage of measurements made on calcite particles for which absorption at visible and near-IR wavelengths can be assumed negligible [*Lindberg*, 1975; *Sokolik and Toon*, 1999]. In this study, however, we did not observe a negative offset in the near IR. This indicates that our samples exhibited significant absorption in that spectral region, which more than compensated for the negative offset produced by the scattering/reflection error. Therefore, in this study, we have chosen to focus our discussion on results obtained without any correction for the scattering/reflection error, which represent conservative (i.e., lower boundary) estimates of absorption. However, for comparison we will also show absorption data obtained with the baseline correction based on measurements with calcite particles described in *Stramski et al.* [2007]. We have not chosen to use this correction routinely because the calcite baseline does not necessarily lead to perfect results for arbitrary particle assemblages, and because our conservative absorption estimates without correction are physically realistic (i.e., positive) across the spectrum including the near IR. Note that the perfect correction for arbitrary particle assemblages whose properties are a priori unknown (as in this study) would be very difficult, if not impossible, to achieve [see *Stramski et al.*, 2007].

[15] For measuring the spectral beam attenuation coefficient of particles, $c_p(\lambda)$, the procedure was similar with the exception of the measurement geometry. In this case the cuvette was placed at a distance of ~25 cm from the entrance port to the integrating sphere. Light stops were aligned within the light path to reduce the cross-section of the beam and the acceptance angle of the detector to less than 1°. No correction was made for light scattered at very small angles within the receiving aperture of the detector. This means that the $c_p(\lambda)$ may be slightly underestimated (on the order of few percent, see *Bricaud et al.* [1983]). The measurements of $c_p(\lambda)$ were made with a 5-nm slit which ensured a desirable increase in the radiant power of the beam with no adverse effect on measuring relatively featureless $c_p(\lambda)$ spectra. All optical measurements were made on optically thin samples with c_p less than 30 m^{-1}. This condition ensured very small or negligible effects of multiple scattering within the 1-cm cuvette [*Stramski and Piskozub*, 2003]. If necessary, the original sample of particle suspension was diluted with filtered seawater for optical measurements. This dilution was accounted for in the calculations of final estimates of $c_p(\lambda)$ and $a_p(\lambda)$ coefficients.

[16] The spectral scattering coefficient of particles, $b_p(\lambda)$, was obtained as a difference $c_p(\lambda) - a_p(\lambda)$, and the single-scattering albedo of particles, $\omega_{op}(\lambda)$, as a ratio $b_p(\lambda)/c_p(\lambda)$. The mass-specific absorption, $a_p{}^*(\lambda)$, and scattering, $b_p{}^*(\lambda)$, coefficients were calculated by normalizing the absorption, $a_p(\lambda)$, and scattering, $b_p(\lambda)$, coefficients to the particle mass concentration, SPM, respectively.

[17] The particle size distribution, PSD, was measured with a Beckman-Coulter Multisizer III equipped with a 100-μm aperture tube. Particle sizing and counting was carried out using 256 size bins increasing logarithmically between the equivalent spherical diameters D of 2 and 60 μm. In order to minimize the coincidence effect (below 5% level), the particle counts were made on suspensions appropriately diluted compared to samples used in the spectrophotometric measurements. This dilution was accounted for in the calculations of final size distributions. These final distributions were obtained from three replicate measurements on samples after subtraction of blank measurements on particle-free seawater (0.2 μm filtrate). Because of the failure of instrument, we do not report on particle size data for the last three samples of the experiment, which were collected in January and February 2006.

2.3. Imaginary Part of Refractive Index

[18] Our estimates of imaginary refractive index have been derived with a procedure described in *Stramski et al.* [2007] and summarized below. Assuming that the mixture of pure water and particles satisfies the Biot-Arago mixing rule, the bulk absorption coefficient of the mixture can be written as [e.g., *Lindberg et al.*, 1999]:

$$a(\lambda) = a_{\mathrm{pm}}(\lambda)\frac{V_{\mathrm{p}}}{V} + a_{\mathrm{w}}(\lambda)\frac{V_{\mathrm{w}}}{V} \tag{1}$$

where $a_{pm}(\lambda)$ is the absorption coefficient of the material forming the particles, $a_w(\lambda)$ is the absorption coefficient of pure water, V_p and V_w are the volumes occupied by particles and water respectively, and $V = V_p + V_w$. The volume fractions are defined as $V'_p = V_p/V$ and $V'_w = V_w/V$, so that $V'_p + V'_w = 1$. The coefficient $a_{pm}(\lambda)$ is a fundamental property of a particulate material related to imaginary refractive index and should not be confused with the absorption coefficient of particles in suspension, $a_p(\lambda)$. We calculated $a_{pm}(\lambda)$ from our spectrophotometric determinations of $a_p(\lambda)$, the estimates of V'_p from particle size measurements, and the values of $a_w(\lambda)$ from the literature [see *Stramski et al.*, 2007]:

$$a_{\mathrm{pm}}(\lambda) = \frac{a_{\mathrm{p}}(\lambda)}{V'_{\mathrm{p}}} + a_{\mathrm{w}}(\lambda) \tag{2}$$

[19] The volume fraction of particles, V'_p, was calculated by integrating the measured size distributions expressed in terms of particle volume concentration, $F_V(D)$. In our experiment, the integration over the range of measured particle sizes (D = 2 to 60 μm) would underestimate total V'_p, primarily because of the missing contribution from small particles ($D < 2$ μm), which were not counted with Coulter Multisizer. As shown below in section 3.1, the $F_V(D)$ distributions for our samples exhibit a characteristic decrease of particle volume concentration with decreasing particle diameter for $D < 4-6$ μm. On the basis of this feature, we made a linear extrapolation of $F_V(D)$ from the measured value of $F_V(D)$ at D = 2 μm to zero at D = 0.01 μm. The contribution of the extrapolated portion of $F_V(D)$ to total V'_p was relatively small and ranged from 2% to 10% (on average 5%). As a result, the possible error in our final estimate of V'_p due to an error in estimated contribution from small particles (<2 μm) is not expected to be significant. We also note that the measured $F_V(D)$ suggest negligible contribution of particles larger than 60 μm to the total particle volume concentration, so the upper detection limit in our measurements at D = 60 μm poses no problem for the estimation of V'_p.

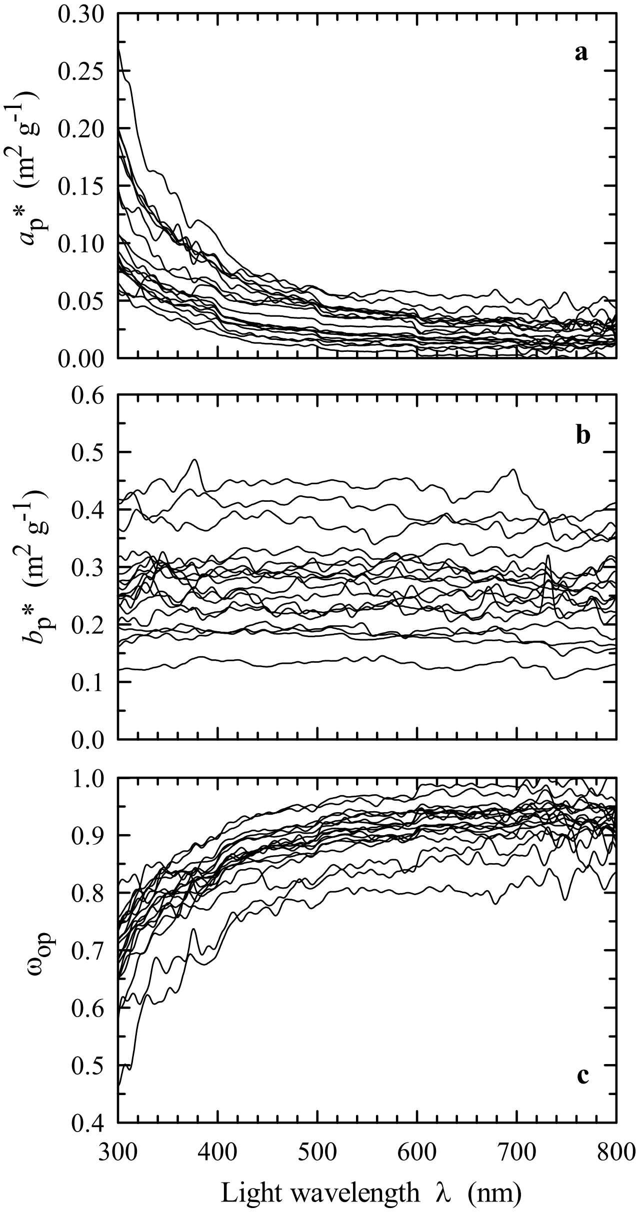

Figure 1. Spectra of (a) mass-specific absorption coefficient $a_p*(\lambda)$, (b) mass-specific scattering coefficient $b_p*(\lambda)$, and (c) single-scattering albedo $\omega_{op}(\lambda)$ for 18 samples of atmospheric particles suspended in seawater examined in this study.

[20] Knowing $a_{pm}(\lambda)$ from equation (2), the imaginary part of refractive index of particles was calculated from:

$$n'(\lambda) = \frac{a_{pm}(\lambda) \times \lambda}{4\pi} \quad (3)$$

Note that a simple way to convert n' to the imaginary index relative to water (reported occasionally in oceanographic literature) is to divide the values from equation (3) by 1.34 (where 1.34 is assumed to represent the real part of refractive index of water for the wavelength range considered). Note also that the estimates of $n'(\lambda)$ from equation (3) should be interpreted with caution as approximate lower limit values of the imaginary index for the examined particulate assemblages. This is because $a_p(\lambda)$, and hence our estimates of $a_{pm}(\lambda)$ and $n'(\lambda)$, are affected by the package effect [*Morel and Bricaud*, 1981; *Stramski et al.*, 2007]. Below we will show the $n'(\lambda)$ spectra for 15 samples, for which both $a_p(\lambda)$ and PSD measurements were made.

2.4. Radiative Transfer Simulations

[21] To estimate the potential influence of atmospheric particles deposited in the ocean on remote sensing reflectance of the ocean, we performed numerical simulations with a Hydrolight (version 4.1) radiative transfer model [*Mobley*, 1994; *Mobley and Sundman*, 2000]. Our calculations were carried out in the spectral range from 350 to 700 nm with a 10-nm interval and included Raman scattering by water molecules. The boundary conditions and the inherent optical properties (IOPs) of the water column were modeled using the library of subroutines provided with the Hydrolight model. The surface boundary conditions assumed clear sky with the Sun zenith angle of 30° and the sea-surface roughness corresponding to a wind speed of 5 m s^{-1}. The ocean was assumed to be infinitely deep and optically homogeneous.

[22] We made two sets of Hydrolight simulations. In the first set of simulations, the spectral absorption, $a(\lambda)$, and scattering, $b(\lambda)$, coefficients were derived from bio-optical models included in the Hydrolight code. Specifically, $a(\lambda)$ was described as the sum of three components: pure seawater [*Pope and Fry*, 1997; *Sogandares and Fry*, 1997], suspended particles, and colored dissolved organic matter [*Prieur and Sathyendranath*, 1981; *Morel*, 1991]. The spectral scattering coefficient was represented as the sum of two components, pure seawater and suspended particles [*Gordon and Morel*, 1983]. The scattering phase function was taken as the sum of contributions by pure water and particles [*Mobley*, 1994]. The particulate contribution represents a "typical" particle phase function based on averaging Petzold's data as described in *Mobley* [1994]. In the second set of Hydrolight simulations, we additionally added one more component, i.e., particles derived from atmospheric deposition referred to as atmospheric particles. The concentration and the average mass-specific absorption and scattering coefficients for atmospheric particles used in these simulations were derived from our experiments and the data reported in the literature, as described below in section 3.3. We caution that while the radiative transfer simulations are intended to provide example results of potential effect of atmospheric particles on remote sensing reflectance using our particular set of input data characteristic of dry deposition in the Southern California coastal region, they are not meant to be generally representative of aerosol deposition effects over the world's oceans where there exists a significant variability in atmospheric particle properties and deposition fluxes associated with both dry and wet deposition.

3. Results and Discussion

3.1. Particle Optical Properties and Size Distributions

[23] The spectra of the mass-specific absorption, $a_p*(\lambda)$, and the mass-specific scattering, $b_p*(\lambda)$, coefficients of atmospheric particles are presented in Figures 1a and 1b.

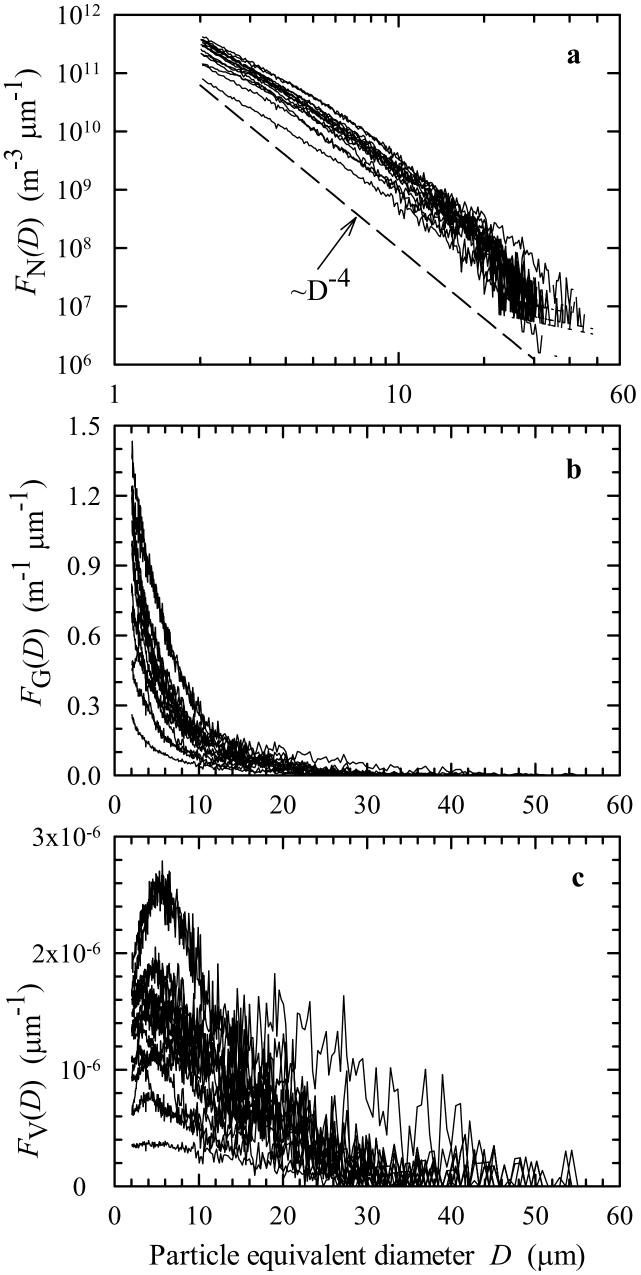

Figure 2. Size distributions for (a) particle number concentration $F_N(D)$, (b) particle projected-area concentration $F_G(D)$, and (c) particle volume concentration $F_V(D)$ for 15 samples of atmospheric particles suspended in seawater examined in this study. For comparison, the slope of −4 for Junge-type particle size distribution is shown in Figure 2a. The size distributions are presented as density functions normalized to the width of particle diameter bins of the Beckman-Coulter instrument (i.e., per micrometer). Note an increased “noise” associated with lower particle counts at larger diameters.

We note that the small-scale features seen in the spectra cannot be interpreted as meaningful features. This “noise” arises mainly from fluctuations in local concentration of particles (primarily relatively rare large particles) within a small volume of sample illuminated by the beam during the spectral scan. Regardless of this noise, the $a_p*(\lambda)$ and $b_p*(\lambda)$ coefficients clearly exhibit significant variation among the samples. As could be expected, the absorption of particles decreases with wavelength (Figure 1a). One important result is that there is still significant absorption in the near-infrared spectral region. In the 780–800 nm region, the average value of a_p* based on all samples is 0.022 m^2 g^{-1}, and in extreme case the a_p* is as high as 0.05 m^2 g^{-1}. We recall that these absorption values represent conservative estimates as they were not corrected for the scattering/reflection error as discussed above. If the calcite-based correction described in *Stramski et al.* [2007] was applied to our data, the absorption estimates in the near IR would be higher on average by 40%, and by a smaller percentage at shorter wavelengths where absorption is higher.

[24] The mass-specific scattering coefficient shows essentially no spectral dependence for the samples examined (Figure 1b). This result is consistent with the particle size data shown in Figure 2, which indicate a considerable contribution of relatively large particles. The $b_p*(\lambda)$ values are relatively small, less than 0.5 m^2g^{-1}. Such low values of $b_p*(\lambda)$ are also consistent with the importance of relatively large particles present in the examined samples [see *Babin et al.*, 2003; *Woźniak and Stramski*, 2004]. The combination of significant absorption with relatively low scattering results in the relatively low values of single-scattering albedo, $\omega_{op}(\lambda)$, which are often less than 0.9 over the large portion of the spectrum and less than 0.8 in the blue for some samples (Figure 1c).

[25] The size distributions of particle number concentration, $F_N(D)$, exhibit a typical decrease in particle concentration with increasing particle equivalent diameter, D (Figure 2a). The slope of $F_N(D)$ on a log-log scale tends to become steeper with increasing D, so the use of a power law with a single slope, for example −4, would not be appropriate over the entire size range. Although the number concentration decreases rapidly with D, the contribution of relatively large particles (>10 μm) to the measured optical properties of our samples is expected to be significant. This expectation is supported by the particle size distributions expressed in terms of the concentration of particle projected area $F_G(D)$ (Figure 2b) and particle volume, $F_V(D)$ (Figure 2c). For example, the median particle diameter, D_{V50}%, which divides the $F_V(D)$ distribution into two equal portions within the range of measurement 2–60 μm, varies from about 8.5 to 18.5 μm in our data set. These variations in D_{V50}% can serve as a simple proxy for variations in the shape of PSD.

[26] The relationships between the mass-specific optical coefficients and particle size are not easily discernible in our data set, especially for the absorption (Figure 3). This is certainly due in part to variations in the composition of various particulate species present in our samples. Another possible reason that may obscure such relationships is that our particle size measurements were made within the restricted range 2–60 μm, whereas the measured optical properties are most likely subject to considerable and variable contribution of particles <2 μm (particles >60 μm appear to play negligible role in our samples). Nevertheless, the general trends of the decrease in $a_p*(\lambda)$ and $b_p*(\lambda)$ with increasing particle size can be seen at least for a portion of our data set. For example, the relatively high values of a_p*

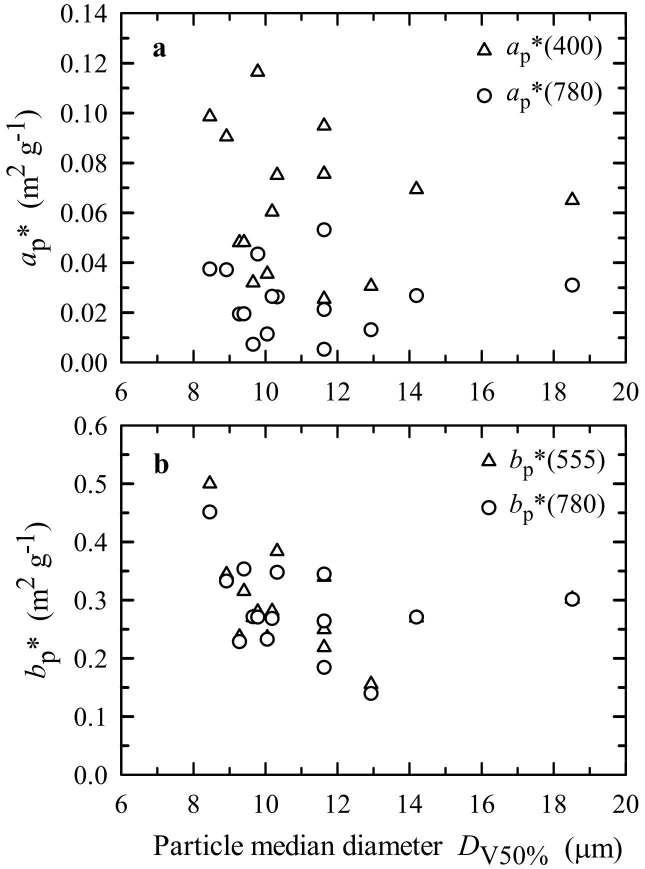

Figure 3. Relationships between the median particle diameter D_{V50}% and (a) mass-specific absorption coefficient a_p* at selected wavelengths of 400 and 780 nm and (b) mass-specific scattering coefficient b_p*(λ) at 555 and 780 nm for samples of atmospheric particles suspended in seawater.

are observed at the lowest values of the median particle diameter, D_{V50}% (Figure 3a). The b_p* data show a clear trend of decrease with increasing D_{V50}%, with the exception for the data point corresponding to the largest value of D_{V50}% (Figure 3b).

[27] Figure 4 compares the optical properties of atmospheric particles suspended in seawater from the present study with results for a few other samples of atmospheric particles suspended in seawater recently reported in the literature. The present samples will be referred to as SD samples or SD atmospheric particles (where SD stands for San Diego). For the SD particles, Figure 4 shows the average spectra based on the 18 samples examined in this study. Other samples in this comparison include the Asian dust sample collected on the cruise in the Japan/East Sea by dry deposition during dust event (sample JES from *Stramski et al.*, 2004b), two Saharan dust samples collected during Saharan dust wet deposition (red rain) event in southern France (samples SAH_1 and SAH_2 from *Stramski et al.*, 2007), and the atmospheric dust sample collected in San Diego during weak rain at the end of Santa Ana event (sample SAN_1 from *Stramski et al.*, 2007). The samples SAH_1 and SAH_2 differ from one another in terms of particle size distribution but they originate from the same original

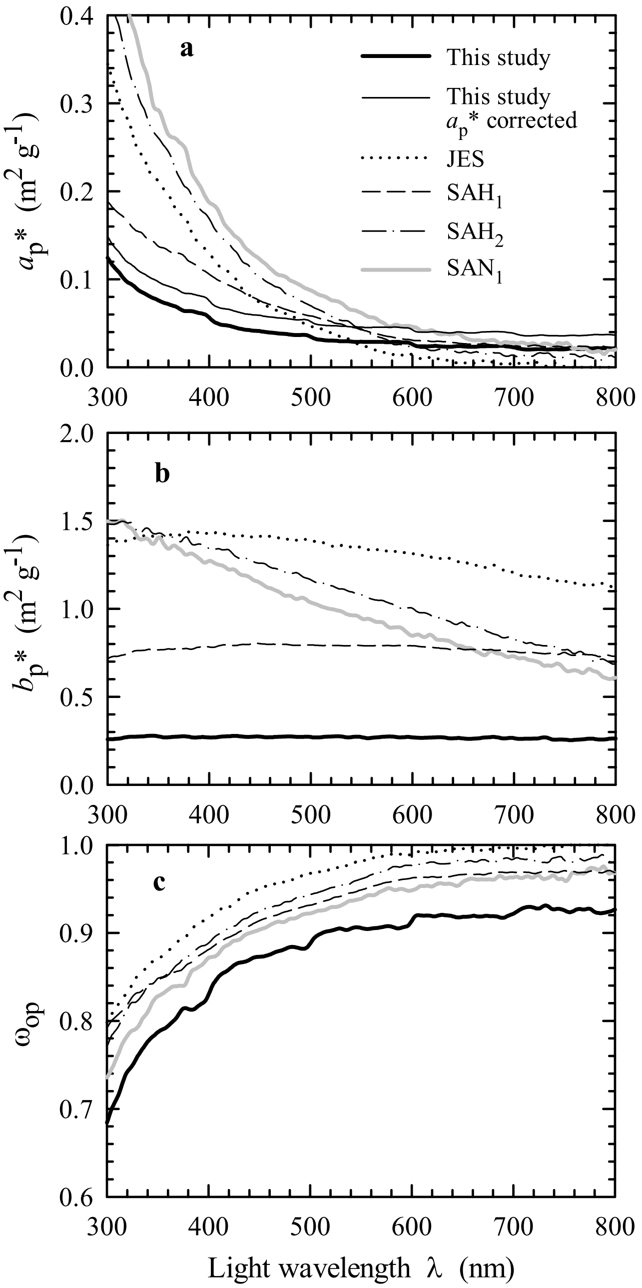

Figure 4. Comparison of the inherent optical properties of atmospheric particles suspended in seawater determined in this study (i.e., average spectra based on 18 samples presented in Figure 1), with similar determinations made on other assemblages of atmospheric particles in earlier studies. Data from the literature represent the atmospheric particles collected by dry deposition in the Japan/East Sea (JES) [*Stramski et al.*, 2004b]; Saharan dust samples collected during red rain event in southern France, SAH_1 and SAH_2; and atmospheric dust sample collected in San Diego during weak rain at the end of Santa Ana event [*Stramski et al.*, 2007]. Spectra of (a) mass-specific absorption coefficient, (b) mass-specific scattering coefficient, and (c) single-scattering albedo of atmospheric particles are shown. In addition, Figure 4a includes the absorption spectrum of particles from this study after correction of absorption measurement for scattering/reflection error (see text for details).

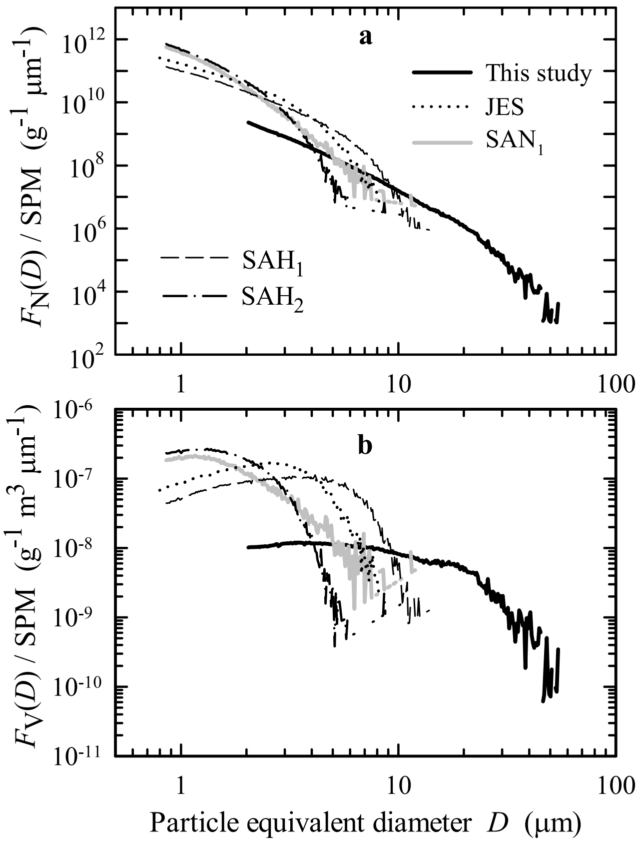

Figure 5. As in Figure 4 but the comparison is presented for the shape of particle size distribution, specifically, the (a) particle number concentration $F_N(D)$ normalized to SPM and the (b) particle volume concentration $F_V(D)$ normalized to SPM. Data for this study represent averaging of 15 sample distributions presented in Figure 2.

sample of Saharan dust (for details see *Stramski et al.* [2007]).

[28] In addition to differences associated with the origin and particulate composition, the samples compared in Figure 4 also differ in terms of particle size distribution (Figure 5). The SD samples contain significantly more large particles compared to the remaining samples. The primary explanation is that large, rapidly sinking particles were removed by settling from samples JES, $\mathrm{SAN_1}$, $\mathrm{SAH_1}$ and $\mathrm{SAH_2}$ prior to measurements [*Stramski et al.*, 2004b, 2007]. Those studies focused on characterizing particle populations dominated by small particles (generally less than 10 μm) that have the potential for relatively long residence times in the upper water column, and for transport over longer distances over the oceans than populations of larger particles. In the present study, the SD samples were not subject to the settling pretreatment, so they are characterized by a much greater proportion of large particles. Particle size distributions (PSDs), which are normalized to SPM for the purpose of comparison, show that the average PSD of SD particles is clearly shifted toward larger particles compared to the PSDs of $\mathrm{SAH_1}$, $\mathrm{SAH_2}$, JES, and $\mathrm{SAN_1}$ samples (Figure 5). For example, the average PSD of SD particle populations points to significant presence of particles >10 μm, which is not the case for other samples. This relatively high contribution of large particles in SD samples is consistent with the collection of our samples in the coastal region via dry deposition.

[29] A decrease of absorption with wavelength for the SD atmospheric particles is less steep than that for other samples shown in Figure 4a. The spectral absorption of SD particles varies approximately as $\lambda^{-1.7}$. Other samples show stronger wavelength dependence, for example $\lambda^{-2.4}$ for $\mathrm{SAH_1}$ and $\lambda^{-4.1}$ for $\mathrm{SAH_2}$. Because the difference between $\mathrm{SAH_1}$ and $\mathrm{SAH_2}$ can be attributed primarily to differences in particle size distribution between these two samples, and not particulate composition (Figure 5, see also *Stramski et al.* [2007]), the package effect for $\mathrm{SAH_1}$ sample is stronger because of the presence of more larger particles than in the $\mathrm{SAH_2}$ sample. Hence the spectrum of $a_p^*(\lambda)$ for $\mathrm{SAH_1}$ is flatter with lower magnitude at ultraviolet (UV) and blue wavelengths compared to $\mathrm{SAH_2}$. The average size distribution for SD atmospheric particles is characterized by much greater contribution of relatively large particles than other samples (Figure 5), so the strongest package effect among the compared samples is actually expected for SD particles. Although it is impossible to determine the extent to which size-induced package effect forces the differences in the $a_p^*(\lambda)$ spectra in Figure 4a, we suppose that this effect is partly responsible for the fact that the SD particles exhibit relatively weak wavelength dependence and relatively low magnitude of $a_p^*(\lambda)$ at UV and blue wavelengths compared to other samples.

[30] In addition to particle size distribution, the differences in the composition of particulate matter can be an important cause of differences in $a_p^*(\lambda)$. Variations in the amounts of iron-rich mineral dust, organic compounds, and black carbon (BC) are recognized as significant sources of variability in aerosol absorption properties [e.g., *Dubovik et al.*, 2002; *Schuster et al.*, 2005; *Bond and Bergstrom*, 2006]. BC is generally considered the most efficient absorbing aerosol species with relatively weak spectral dependence characterized by a gradual decrease of absorption with wavelength and still significant absorption in the near IR [e.g., *Lindberg et al.*, 1993; *Kirchstetter et al.*, 2004]. Other major aerosol absorbing substances exhibit stronger spectral dependence than BC. Iron oxides, which are a common component in most mineral dust, show strong absorption in the UV and blue wavelengths and a distinct transition to weak absorption at approximately 500–600 nm [*Lindberg et al.*, 1993; *Sokolik and Toon*, 1999]. The absorption of organic aerosol substances has a maximum at ultraviolet wavelengths but the absorption tail typically extends to visible wavelengths and becomes insignificant in the near IR [*Jacobson*, 1999; *Kirchstetter et al.*, 2004]. We have no chemical analysis available for our SD samples but the sampling site and long period of sample collection suggests a complex composition that includes those major groups of absorbing aerosol substances. It is also noteworthy that the SD particles have relatively high absorption at red and near-IR wavelengths. This feature is reinforced if we consider our estimates of $a_p^*(\lambda)$ obtained upon scattering/reflection correction, which are higher on average by 40% than the uncorrected $a_p^*(\lambda)$ in the near IR. The corrected spectra of SD particles have clearly the highest values of $a_p^*(\lambda)$ at wavelengths >650 nm (i.e., $a_p^* \approx 0.037–0.04\ m^2\ g^{-1}$) among the samples compared in Figure 4a.

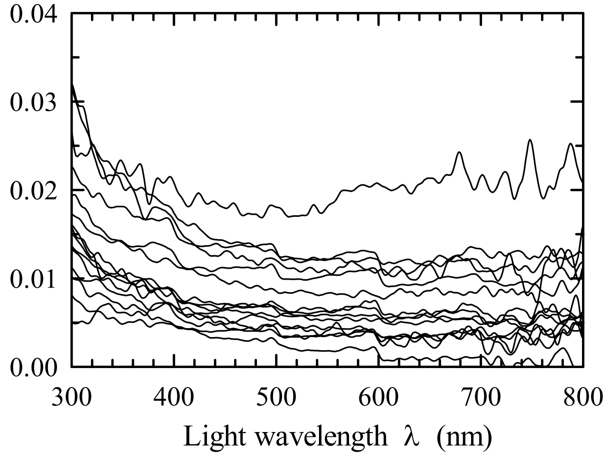

Figure 6. Spectra of the imaginary part of the refractive index of the atmospheric particles examined in this study. The n' spectra are presented for 15 samples for which both absorption and particle size distribution measurements were made.

[31] The mass-specific scattering coefficient, $b_p*(\lambda)$, for SD atmospheric particles displays significantly lower values than the other samples shown in Figure 4b. The $b_p*(\lambda)$ spectrum for SD particles is virtually flat. These results can again be explained by relatively high contribution of large particles in SD samples. We also note that the relatively low average value of b_p* of about 0.27 m^2 g^{-1} for SD particles is consistent with predictions of Mie scattering theory for hypothetical particle populations having a broad size distribution whose slope is close to or less steep than −4 and the refractive index is relatively high within the range typical of mineral particles [*Babin et al.*, 2003; *Woźniak and Stramski*, 2004].

[32] As a consequence of results presented in Figures 4a and 4b, the average values of the single-scattering albedo, $\omega_{op}(\lambda)$, of SD particles are significantly lower than those for other samples of atmospheric particles in this comparison (Figure 4c). Over the large portion of the spectrum, $\omega_{op}(\lambda)$ of SD particles is less than or about 0.9. Specifically, $\omega_{op}(\lambda)$ is less than 0.91 for $\lambda < 600$ nm, less than 0.9 for $\lambda < 510$ nm, and <0.83 for $\lambda < 400$ nm (note that these values would be lower if we used the absorption estimates after correction for scattering/reflection effects in our measurement system). Whereas our data describe the properties of atmospheric aerosols suspended in seawater, it is noteworthy that the determinations of single-scattering albedo of aerosols in air are of great interest to studies of radiative forcing at the Earth's surface, within the atmosphere, and at the top of the atmosphere (TOA). For example, aerosols have a net negative TOA forcing (a cooling effect) when $\omega_{op} > 0.95$, a net positive TOA forcing (a warming effect) for $\omega_{op} < 0.85$, and for the intermediate values of ω_{op} the net effect can change from negative to positive forcing depending on other factors [*Ramanathan et al.*, 2001]. From Figure 4c we see that the assemblages of atmospheric particles upon their suspension in seawater cover this critical range of single-scattering albedo.

[33] Figure 6 shows variability in our estimates of imaginary refractive index, $n'(\lambda)$, for 15 samples of atmospheric particles. Although these estimates must be interpreted with caution as approximate lower limit of $n'(\lambda)$ due to the package effect, the variability in $n'(\lambda)$ provides useful information because it reflects mainly the variations in the composition of absorbing substances between the samples. There is about one order of magnitude variation between the lowest and highest estimates of $n'(\lambda)$ for our samples. For example, at $\lambda = 400$ nm, n' ranges from about 0.0047 to 0.021. In the near-IR wavelengths close to 800 nm, the n' estimates are as high as 0.012–0.014, with the exception of one sample for which n' exceeds 0.02. We recall that we report here on the n' values in vacuo, and not relative to water. The values relative to water are reduced by a factor of about 1.34.

[34] It is instructive to make comparison of our estimates with other data on $n'(\lambda)$ of atmospheric particles. Our estimates in Figure 6 fall within a broad range of values reported in the literature [*Gillespie and Lindberg*, 1992; *Sokolik et al.*, 1993]. For example, diffuse reflectance measurements for atmospheric dust samples collected in several regions, including highly populated urban areas and desert areas, showed considerable variation in the bulk imaginary refractive index of the samples [*Gillespie and Lindberg*, 1992]. The higher values on the order of 10^{-2} were observed in urban or industrialized areas where the effects of anthropogenic contributions are significant. The lower values, generally on the order of 10^{-3} but extending to >0.01, were observed in less populated rural areas with less pollution. Similar ranges and patterns of variability were retrieved from ground-based measurements of sun and sky radiances in various regions [*Dubovik et al.*, 2002]. Relatively high values of n' exceeding 0.01 were reported for urban/industrial and biomass burning aerosols. For aerosol type referred to as desert dust, the retrieved values of n' were significantly lower, decreasing from ∼0.0025–0.003 at blue wavelengths to ∼0.001 or less in the near-IR spectral region. In contrast, however, significantly higher values of n' were determined for Saharan aerosols from diffuse reflectance measurements on samples from several locations in the Atlantic [*Patterson et al.*, 1977]. The values obtained by *Patterson et al.* [1977] decrease from ∼0.02 in the UV and 0.01 in the blue to ∼0.003–0.004 in the red. The determinations of n' for the SAH_1 sample by *Stramski et al.* [2007] are between the relatively high estimates for Saharan dust obtained by *Patterson et al.* [1977] and the relatively low estimates for desert dust derived by *Dubovik et al.* [2002].

[35] The variability of n' for the bulk atmospheric particulate matter can be explained in terms of certain important categories of materials that make up the particulate matter. The bulk of this matter is generally composed of weak absorbers in the visible and near IR such as quartz, calcite, silicate clay minerals, sulfates, and sea salt particles. These materials have negligible or very low imaginary index less than 10^{-3} at relevant wavelengths [*Lindberg*, 1975; *Lindberg et al.*, 1993; *Sokolik and Toon*, 1999]. Added to this mixture are small (but highly variable) amounts of strong absorbers, such as iron oxides typically associated with mineral dust, and black carbon (BC) from biomass burning and combustion of fossil fuels. In the atmospheric literature the estimates of $n'(\lambda)$ for BC span the range from about 0.44 to over 1, which is orders of magnitude higher

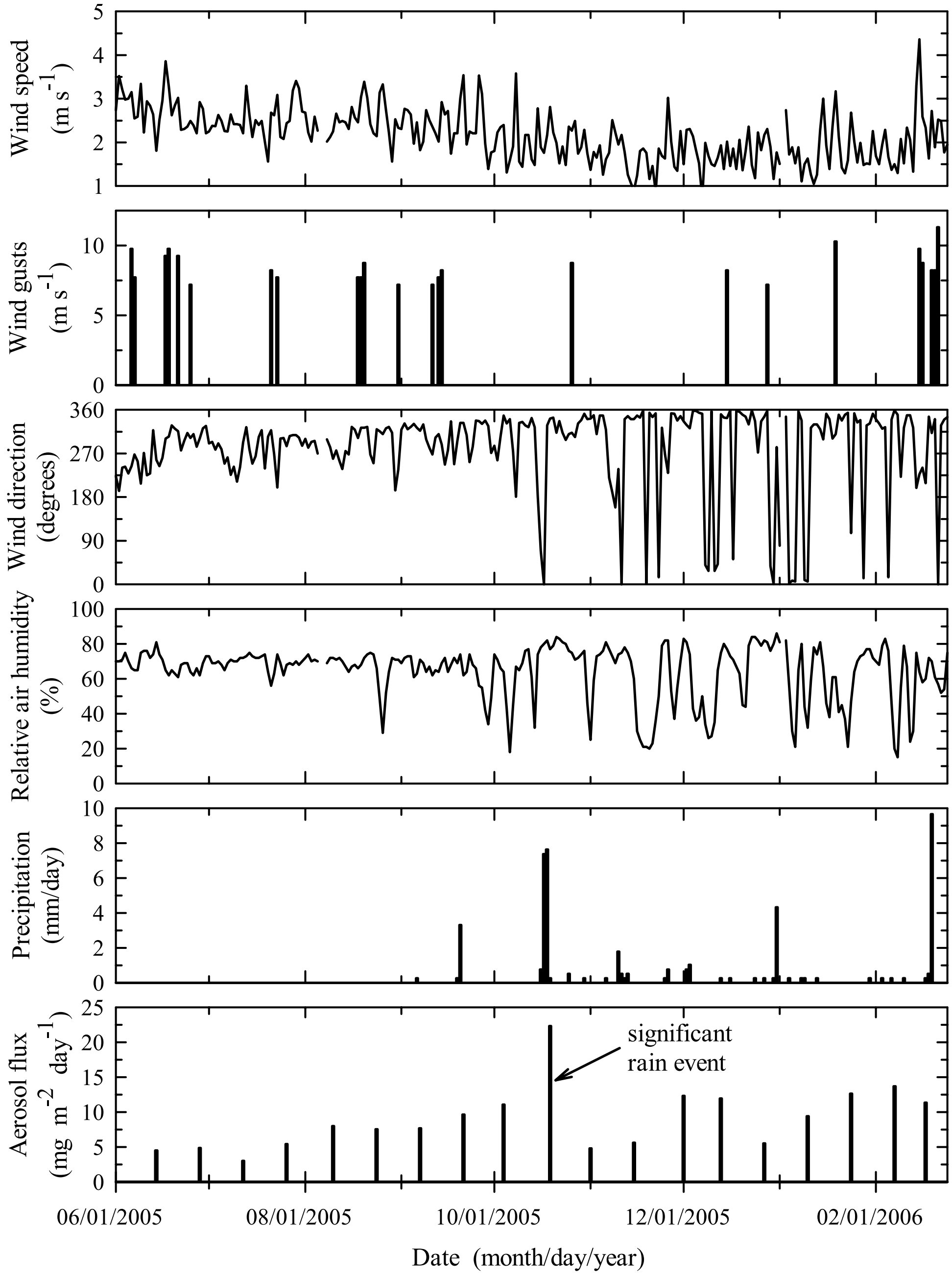

Figure 7. Time series of wind speed, wind gusts, wind direction, relative air humidity, precipitation, and average aerosol deposition flux at our study site. Aerosol flux determination based on samples collected during a period with significant precipitation in October 2005 is indicated by an arrow. The time series represent the duration of the experiment, in which the sample collection started on 18 May 2005 and ended on 17 February 2006. The first five panels represent daily averages, and the last panel represents approximately a 4-week average data.

than $n'(\lambda)$ for other most common particulate substances [e.g., *Lindberg et al.*, 1993; *Schuster et al.*, 2005; *Bond and Bergstrom*, 2006]. Therefore BC can be a highly significant or dominant absorber in aerosols at visible and near-IR wavelengths [e.g., *Rosen et al.*, 1978; *Yasa et al.*, 1979; *Sato et al.*, 2003]. Certain amounts of oxides of iron are often present in atmospheric dust [e.g., *Arimoto et al.*, 2002]. The $n'(\lambda)$ values for these oxides are comparable to those of BC in the UV and blue wavelengths but, in contrast to BC, iron oxides make a transition to weak absorption within the wavelength range 500–600 nm [*Lindberg et al.*, 1993; *Sokolik and Toon*, 1999]. The values of $n'(\lambda)$ for organic carbon aerosols appear to be less well documented. *Sato et al.* [2003] reported the values decreasing from about 0.03 at 400 nm to 0.005 at near-IR wavelengths.

[36] In summary, our data in Figure 6 and the overview of the literature data on n' for atmospheric particulate matter suggest that BC can be a significant absorption component

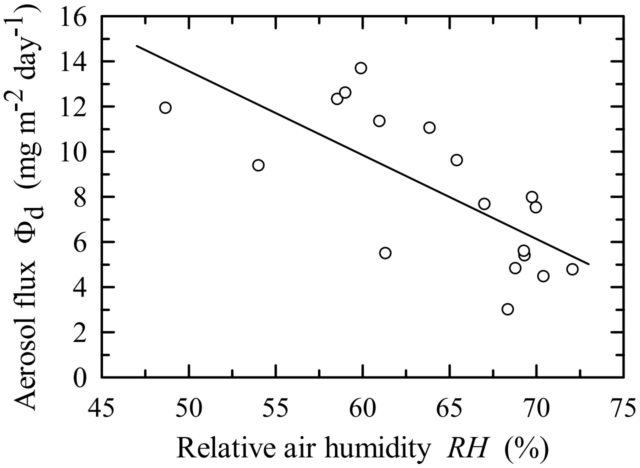

Figure 8. Relationship between the relative humidity of air RH averaged over the period when aerosol samples were collected (~4 weeks) and the average aerosol deposition flux Φ_d. The best fit linear regression is $\Phi_d = 0.372$ RH − 32.178, where the coefficient of determination r^2 is 0.52, and the number of observations is 18.

in our samples. The variability among the samples presented in Figure 6 indicates that BC is mixed with other, both absorbing and nonabsorbing or weakly absorbing, aerosol species in variable proportions. The significant role of BC is especially evident for the samples that have high n' in the near IR as other aerosol species cannot produce such absorption signal. Naturally this conclusion is also applicable to the data of the mass-specific absorption coefficient presented in Figures 1a and 4a, which show significant absorption in the near IR.

3.2. Aerosol Deposition Flux and Meteorological Conditions

[37] Figure 7 shows time series of aerosol deposition flux along with the selected meteorological parameters during our experiment. The 4-week average value of dry aerosol deposition flux, Φ_d, exhibits more than fourfold variation between 3 and 13.7 mg m^{-2} day^{-1} over the period of the experiment. On one occasion when the period of particle collection included a significant rain event (October 2005), the estimates of the deposition rate reached ~23 mg m^{-2} day^{-1}. As noted above, no optical and size measurements were made for that sample.

[38] Because of the 4-week period of sample collection and associated averaging of aerosol deposition flux, we generally expect no significant relationship between deposition rates and weather conditions that vary on shorter time scales. The only atmospheric parameter that has shown significant correlation with dry deposition flux in our data set is relative humidity of air averaged over the same period as the aerosol sample collection (Figure 8). Low air humidity (during time periods without precipitation) is generally associated with higher deposition fluxes. This result is likely a manifestation of the influences of Santa Ana conditions on our data set. Santa Ana is a local weather condition that occurs in Southern California mainly in the fall and winter, and may last several days. The formation of Santa Ana wind is associated with an intense high-pressure system in the Great Basin (in Nevada and Utah regions) and a weak low-pressure system off the southern California coast [*Sommers*, 1978; *Raphael*, 2003]. The resultant strong pressure gradient produces significant winds that can pick up surface dust from arid areas and carry it westward over the coastal ocean. Such dust plumes spreading toward the Southern California Bight during Santa Ana have been observed in satellite images [*Hu and Liu*, 2003]. The fall and winter seasons 2005/2006 at our sampling location included Santa Ana events with characteristic low air humidity. Time series in Figure 7 show that the daily average air humidity decreased below 40% on several occasions with the most pronounced event in November 2005 when air humidity of 20–25% persisted for 5 days. However, because our sampling period was significantly longer than a typical Santa Ana event, our samples represent mixed conditions rather than particles associated solely with Santa Ana events.

3.3. Potential Implications for Ocean Optics and Ocean Color Remote Sensing

[39] The approximate contribution of aerosol deposition to ocean optical properties can be assessed by combining our optical data of SD atmospheric particles suspended in seawater, estimates of aerosol deposition rates, and the general knowledge of the optical properties of seawater. The 4-week average dry deposition rate of aerosols in our experiment varied between $\Phi_d \approx 3.0$ and 13.7 mg m^{-2} d^{-1}. In our calculations we will assume a rather extreme situation of intense deposition event when the aerosol flux reaches 78 mg m^{-2} d^{-1} and persists for 5 days. The estimate of 78 mg m^{-2} d^{-1} is based on a proportionality between aerosol concentration in air and aerosol deposition rate. The air pollution data for the Southern California region indicate that the average concentration of aerosols less than 10 micrometers in diameter (PM10) at San Diego sites is generally below 30 μg m^{-3} (California Air Resources Board, http://www.arb.ca.gov/aqd/aqdpage.htm). However, concentrations of 160 μg m^{-3} or higher were observed in coastal areas of southern Los Angeles several times in recent years and concentrations as high as 180 μg m^{-3} were observed in 2003 at an Escondido site north of San Diego. These high concentrations are 5–6 times higher than typical concentrations. Therefore our assumption that the deposition flux of 78 mg m^{-2} d^{-1} (i.e., ~5.7 times the maximum 4-week average flux observed during our experiment) persists for 5 days may represent an extreme deposition event within the urban coastal areas of Southern California.

[40] In our calculations we also assume that the concentration of atmospheric particles after the deposition event is uniform within the oceanic mixed layer down to a depth of 10 m and that no particle losses from the mixed layer occurred during the 5-day event. With these assumptions, after 5 days of deposition, we obtain the mass concentration of 39 mg m^{-3} of atmospheric particles within the ocean mixed layer. The product of this concentration and our average mass-specific coefficients $a_p^*(\lambda)$ and $b_p^*(\lambda)$ taken from Figures 4a and 4b yields the absorption, $a_p(\lambda)$, and scattering, $b_p(\lambda)$, coefficients produced by these atmospheric particles suspended in seawater. For example, at 400 nm we obtain $a_p(400) \approx 0.0022$ m^{-1} and $b_p(400) \approx 0.011$ m^{-1}. The estimated absorption $a_p(400)$ is about 3 times smaller than pure water absorption a_w at 400 nm,

which is about 0.0066 m^{-1} [*Pope and Fry*, 1997]. At longer wavelengths this comparison would favor a_w even more because a_p decreases and a_w increases with wavelength. The estimated scattering $b_p(400)$ is, however, higher by about 40% than pure seawater scattering b_w at 400 nm, which is about 0.0076 m^{-1} [*Smith and Baker*, 1981]. At longer wavelengths this comparison would favor b_p even more because our estimates of b_p are spectrally flat and b_w decreases with wavelength.

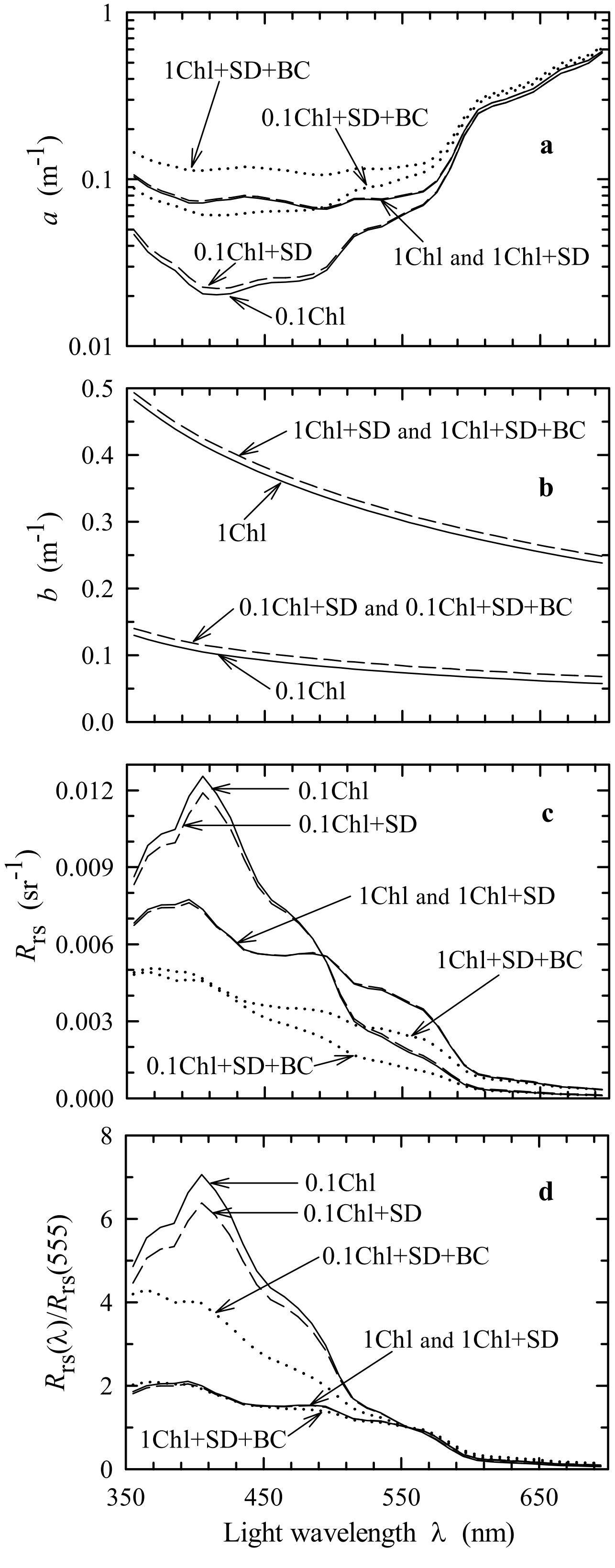

Figure 9. (a) Spectral total absorption coefficients $a(\lambda)$ for hypothetical water samples representing Case 1 water body with chlorophyll *a* concentration of 0.1 and 1.0 mg m^{-3} (denoted as 0.1Chl and 1Chl, respectively), for the same Case 1 water samples with the addition of 39 mg m^{-3} of SD atmospheric particles examined in this study (denoted as 0.1Chl + SD and 1Chl + SD), and for the same Case 1 water samples with the addition of 39 mg m^{-3} of atmospheric particles enriched with black carbon, i.e., the atmospheric particulate assemblage consisting of 90% of SD particles and 10% of black carbon (BC) particles (denoted as 0.1Chl + SD + BC and 1Chl + SD + BC). (b) As in Figure 9a but for the total scattering coefficient $b(\lambda)$. (c) Spectra of remote sensing reflectance $R_{rs}(\lambda)$ obtained from radiative transfer simulations for several cases of inherent optical properties of seawater presented in Figures 9a and b. (d) As in Figure 9c but for the band ratio of remote sensing reflectance $R_{rs}(\lambda)/R_{rs}(555)$.

[41] It is instructive to compare our estimates of $a_p(\lambda)$ and $b_p(\lambda)$ for the considered aerosol deposition event with the estimates of total absorption, $a(\lambda)$, and total scattering, $b(\lambda)$, coefficients predicted from Case 1 bio-optical models built in the Hydrolight code for waters with relatively low and high concentrations of chlorophyll *a*, i.e., Chl = 0.1 mg m^{-3} and Chl = 1 mg m^{-3}, respectively. This comparison shows that the input of SD atmospheric particles would produce generally small or negligible enhancement of total absorption (Figure 9a). The maximum increase would be about 10% in the UV and violet wavelengths at low Chl = 0.1 mg m^{-3}. However, the SD particles would generally have a larger effect on total scattering (Figure 9b). For example, at Chl = 0.1 mg m^{-3}, $b(\lambda)$ would increase by 10% at 400 nm and 18% at 700 nm because of the addition of SD particles. At Chl = 1 mg m^{-3} these effects would be smaller (~2.5 and 4.4%). These contributions of SD particles to total IOPs of seawater have some effect on the spectral remote sensing reflectance, $R_{rs}(\lambda)$, which was calculated with the Hydrolight simulations (Figures 9c and 9d). For example, at low Chl = 0.1 mg m^{-3} the reflectance is somewhat reduced in the blue wavelengths because of the input of SD particles (Figure 9c). As a result, the blue-to-green reflectance ratio, $R_{rs}(440)/R_{rs}(555)$, is reduced by about 7% (Figure 9d). However, at higher Chl these effects on reflectance are negligible.

[42] The above results suggest that an example event in the coastal waters of Southern California with high aerosol deposition flux of 78 mg m^{-2} d^{-1} persisting for 5 days and all atmospheric particles being trapped within the top 10 m layer would produce a sizable effect on ocean reflectance if water turbidity is relatively low such as Case 1 water type with chlorophyll *a* concentration of about 0.1 mg m^{-3}. At higher water turbidities with higher chlorophyll *a* concentration or generally higher concentrations of marine particles which often occur in coastal environments, such a deposition event would generally have negligibly small

impact on ocean reflectance. Naturally, these assessments are constrained by our specific assumptions about the deposition event, especially the assumed magnitude of aerosol flux, duration of the event, depth of mixed layer, and the mass-specific optical coefficients of atmospheric particles. Thus we caution against indiscriminate generalization or extrapolation of these results within a broader environmental context.

[43] One important aspect that has been revealed by the above assessments is that the total absorption coefficient of seawater has been very weakly affected by inputs of atmospheric particles that have the mass-specific absorption determined from our samples of SD particles. Therefore we made additional set of Hydrolight simulations to test the sensitivity of remote sensing reflectance to the deposition of atmospheric particulate assemblage that has higher mass-specific absorption than the SD particles. In this additional set of calculations, all assumptions about the aerosol deposition event remained the same as above. The only difference is that we assumed that the total mass concentration of atmospheric particulate matter consists of 10% of black carbon (BC) particles and 90% of SD atmospheric particles. We assumed that the BC-specific absorption coefficient is 10 m^2 g^{-1} and is wavelength-independent in the spectral range 350–700 nm. The scattering properties of BC-enriched particulate matter remain the same as those for the SD particulate matter. BC can contribute 5–15% to the total aerosol mass concentration in urban regions and the BC-specific absorption ranges between about 5 and 22 m^2 g^{-1} [*Martins et al.*, 1998; *Schuster et al.*, 2005; *Bond and Bergstrom*, 2006]. The observations in industrial areas of Southern California (e.g., Long Beach) showed that BC is a significant component with ~10% contribution to the total aerosol mass concentration in this region [*Solomon et al.*, 1989; *Allen et al.*, 2000]. Therefore our assumptions about the addition of BC appear reasonable for examining the sensitivity of Hydrolight simulations to the deposition of highly absorbing urban aerosols originating from industrial or polluted regions.

[44] With these assumptions, the total absorption coefficient of seawater that contains the BC-enriched atmospheric particulate matter has increased significantly compared to Case 1 waters with no atmospheric particles, for example more than 2.5-fold at Chl = 0.1 mg m^{-3} and 1.5-fold at Chl = 1 mg m^{-3} within the blue wavelength range (Figure 9a). Large changes in the total absorption by seawater because of the deposition of BC-enriched particulate matter make large effect on remote sensing reflectance, which becomes greatly reduced over most of the spectral region (Figure 9c). However, in these simulations the input of BC-enriched particles has an important effect on the blue-to-green reflectance band ratios only at low Chl. At Chl = 1 mg m^{-3}, the effect on the reflectance band ratios is very small (Figure 9d).

4. Concluding Remarks

[45] The characterization of optical properties of atmospheric particles suspended in seawater can aid in an understanding of the question whether atmospheric deposition of particles can have appreciable effects on ocean optical properties. Although many atmospheric studies have addressed the optical properties of aerosols, those studies typically lack direct measurements of absorption and scattering coefficients of aerosols with high spectral resolution over a wide spectral range from ultraviolet to infrared. In addition, the optical properties of aerosols in air are not likely to be representative of the properties after particle deposition in water. In this study, we have presented results obtained with high spectral resolution measurements of absorption and scattering properties within the spectral region from UV through near IR. These measurements were made on atmospheric particles suspended in prefiltered seawater upon their collection by dry deposition at a near-shore location in the Southern California. These measurements in conjunction with radiative transfer simulations provided preliminary assessments which demonstrate that aerosol deposition may have sizable effect on ocean optical properties including remote sensing reflectance under certain scenarios of deposition events, residence times of particles in the water column, and particle properties.

[46] Our work indicates that the potential significance of highly absorbing components of atmospheric particulate matter, especially black carbon (BC), deserves more attention in the study of particle optical properties in marine environments. The ubiquitous presence of BC particles in the atmosphere, ice, rivers, soil, marine sediments, and ultrafiltered estuarine and ocean waters [e.g., *Goldberg*, 1985; *Middelburg et al.*, 1999; *Mannino and Harvey*, 2004] suggests that this material occurs also in marine suspended particulate matter. Mechanisms that introduce BC to the ocean include atmospheric deposition, riverine inputs, and marine engine exhaust.

[47] Further work is needed to elucidate the potential role of BC in particulate absorption of seawater, including the outstanding question of whether marine particulate assemblages absorb near-IR radiation [e.g., *Babin and Stramski*, 2002; *Tassan and Ferrari*, 2003; *Bowers and Binding*, 2006]. These efforts will require the determinations of particulate BC in seawater and improvements in the accuracy of particle absorption measurements taken in situ or on natural seawater samples. In particular, these improvements will require a reduction of errors associated with light scattering, which limit the accuracy of present methods such as filter pad and reflective tube techniques [e.g., *Lohrenz*, 2000; *Zaneveld et al.*, 1994]. These limitations are particularly severe in spectral regions where particulate absorption is weak. Unlike other common particle species, BC may exhibit significant and possibly measurable contribution to the near-IR absorption in seawater, so particle absorption measurements with accuracy higher than presently available may provide a near-IR signature for BC presence in seawater. Whereas the laboratory measurements with a center-mount integrating sphere applied in this study reduce the scattering error efficiently, this method is not suitable to natural seawater samples that have generally low particle concentrations. One technique with prospects for improvements in this area is offered by the integrating cavity absorption meter [e.g., *Röttgers et al.*, 2005]. This technique provides a capability for direct measurement of particle absorption in natural seawater with greatly minimized scattering error, which may prove adequate for exploring the potential BC signature in marine particulate

matter associated with atmospheric deposition or other sources.

[48] **Acknowledgments.** This study was supported by NASA's Earth Science Enterprise Earth Observing System Interdisciplinary Science Program (EOS/IDS, grants NNG04GJ38G and NNG04GK50G awarded to M.S. and D.S.). We thank R. Reynolds for assistance in the laboratory and comments on the manuscript, V. Wright for assistance in the laboratory, and an anonymous reviewer for helpful comments.

References

Allen, J. O., L. S. Hughes, L. G. Salmon, P. R. Mayo, R. J. Johnson, and G. R. Cass (2000), Characterization and evolution of primary and secondary aerosols during $PM_{2.5}$ and PM_{10} episodes in the south coast air basin, in *CalTech Technical Report A-22*, Coordinating Research Council, Alpharetta, Ga.

Antoine, D., and A. Morel (1999), A multiple scattering algorithm for atmospheric correction of remotely sensed ocean color (MERIS instrument): Principle implementation for atmospheres carrying various aerosols including absorbing ones, *Int. J. Remote Sens.*, *20*, 1875–1916.

Arimoto, R., W. L. Balsam, and C. Schloesslin (2002), Visible spectroscopy of aerosol particles collected on filters: Iron-oxide minerals, *Atmos. Environ.*, *36*, 89–96.

Babin, M., and D. Stramski (2002), Light absorption by aquatic particles in the near-infrared spectral region, *Limnol. Oceanogr.*, *47*, 911–915.

Babin, M., and D. Stramski (2004), Variations in the mass-specific absorption coefficient of mineral particles suspended in water, *Limnol. Oceanogr.*, *49*, 756–767.

Babin, M., A. Morel, V. Fournier-Sicre, F. Fell, and D. Stramski (2003), Light scattering properties of marine particles in coastal and open ocean waters as related to the particle mass concentration, *Limnol. Oceanogr.*, *48*, 843–859.

Bond, T. C., and R. W. Bergstrom (2006), Light absorption by carbonaceous particles: An investigative review, *Aerosol Sci. Technol.*, *40*, 27–67.

Bowers, D. G., and C. E. Binding (2006), The optical properties of mineral suspended particles: A review and synthesis, *Estuarine Coastal Shelf Sci.*, *67*, 219–230.

Bowers, D. G., G. E. L. Harker, and B. Stephan (1996), Absorption spectra of inorganic particles in the Irish Sea and their relevance to remote sensing of chlorophyll, *Int. J. Remote Sens.*, *17*, 2449–2460.

Bricaud, A., A. Morel, and L. Prieur (1983), Optical efficiency factors of some phytoplankters, *Limnol. Oceanogr.*, *35*, 562–582.

Bricaud, A., A.-L. Bedhomme, and A. Morel (1988), Optical properties of diverse phytoplanktonic species: Experimental results and theoretical predictions, *J. Plankton Res.*, *10*, 851–873.

Charlson, R. J., J. E. Lovelock, M. O. Andreae, and S. G. Warren (1987), Ocean phytoplankton, atmospheric sulphur, cloud albedo and climate, *Nature*, *326*, 655–661.

Christoforou, C. S., L. G. Salmon, M. P. Hanningan, P. A. Solomon, and G. R. Cass (2000), Trends in fine particle concentration and chemical composition in Southern California, *J. Air Waste Manage. Assoc.*, *50*, 43–53.

Claustre, H., A. Morel, S. B. Hooker, M. Babin, D. Antoine, K. Oubelkheir, A. Bricaud, K. Leblanc, B. Queguiner, and S. Maritorena (2002), Is desert dust making oligotrophic waters greener?, *Geophys. Res. Lett.*, *29*(10), 1469, doi:10.1029/2001GL014056.

Dubovik, O., B. Holben, T. F. Eck, A. Smirnov, Y. J. Kaufman, M. D. King, D. Tanre, and I. Slutsker (2002), Variability of absorption and optical properties of key aerosol types observed in world wide locations, *J. Atmos. Sci.*, *59*, 590–608.

Duce, R. A., C. K. Unni, B. J. Ray, J. M. Prospero, and J. T. Merrill (1980), Long-range atmospheric transport of soil dust from Asia to the tropical North Pacific: Temporal variability, *Science*, *209*, 1522–1524.

Duce, R. A., et al. (1991), The atmospheric input of trace species to the world ocean, *Global Biogeochem. Cycles*, *5*, 193–259.

Gillespie, J. B., and J. D. Lindberg (1992), Seasonal and geographical variations in imaginary index of atmospheric particulate matter, *Appl. Opt.*, *31*, 2107–2111.

Goldberg, E. D. (1985), *Black Carbon in the Environment: Properties and Distribution*, 198 pp., John Wiley & Sons, New York.

Gordon, H. R. (1997), Atmospheric correction of ocean color imagery in the Earth Observing System era, *J. Geophys. Res.*, *102*, 17,081–17,106.

Gordon, H. R., and A. Morel (1983), *Remote Assessment of Ocean Color for Interpretation of Satellite Visible Imagery: A Review*, *Lecture Notes on Coastal and Estuarine Studies*, 114 pp., Springer-Verlag, New York.

Hu, H., and W. T. Liu (2003), Oceanic thermal and biological responses to Santa Ana winds, *Geophys. Res. Lett.*, *30*(11), 1596, doi:10.1029/2003GL017208.

Hughes, L. S., et al. (1999), The size and composition distribution of atmospheric particles in Southern California, *Environ. Sci. Technol.*, *33*, 3506–3515.

Husar, R. B., J. M. Prospero, and L. L. Stowe (1997), Characterization of tropospheric aerosols over the oceans with the NOAA/AVHRR optical thickness operational product, *J. Geophys. Res.*, *102*, 16,889–16,909.

Jacobson, M. Z. (1999), Isolating nitrated and aromatic aerosols and nitrated aromatic gases as sources of ultraviolet light absorption, *J. Geophys. Res.*, *104*, 3527–3542.

Jaffe, D. A., et al. (1999), Transport of Asian air pollution to North America, *Geophys. Res. Lett.*, *26*, 711–714.

Kaufman, Y. J., D. Tanre, and O. Boucher (2002), A satellite view of aerosols in climate system, *Nature*, *419*, 215–223.

Kirchstetter, T. W., T. Novakov, and P. V. Hobbs (2004), Evidence that the spectral dependence of light absorption by aerosols is affected by organic carbon, *J. Geophys. Res.*, *109*, D21208, doi:10.1029/2004JD004999.

Li, S.-M., A. M. Macdonald, J. W. Strapp, Y.-N. Lee, and X.-L. Zhou (1997), Chemical and physical characterizations of atmospheric aerosols over Southern California, *J. Geophys. Res.*, *102*, 21,341–21,353.

Lindberg, J. D. (1975), The composition and optical absorption coefficient of atmospheric particulate matter, *Opt. Quantum Electron.*, *7*, 131–139.

Lindberg, J. D., R. E. Douglass, and D. M. Garvey (1993), Carbon and the optical properties of atmospheric dust, *Appl. Opt.*, *32*, 6077–6081.

Lindberg, J. D., R. E. Douglass, and D. M. Garvey (1999), Atmospheric particulate absorption and black carbon measurement, *Appl. Opt.*, *38*, 2369–2376.

Lohrenz, S. E. (2000), A novel theoretical approach to correct for pathlength amplification and variable sampling loading in measurements of particulate spectral absorption by the quantitative filter technique, *J. Plankton Res.*, *22*, 639–657.

Mannino, A., and H. R. Harvey (2004), Black carbon in estuarine and coastal ocean dissolved organic carbon, *Limnol. Oceanogr.*, *49*, 735–740.

Martin, J. H., et al. (1994), Testing the iron hypothesis in ecosystems of the equatorial Pacific Ocean, *Nature*, *371*, 123–129.

Martins, J. V., P. Artaxo, C. Liousse, J. S. Reid, P. V. Hobbs, and Y. J. Kaufman (1998), Effects of black carbon content, particle size, and mixing on light absorption by aerosols from biomass burning in Brazil, *J. Geophys. Res.*, *103*, 32,041–32,050.

Middelburg, J. J., J. Nieuwenhuize, and P. van Breugel (1999), Black carbon in marine sediments, *Mar. Chem.*, *65*, 245–252.

Mobley, C. D. (1994), *Light and Water. Radiative Transfer in Natural Waters*, 592 pp., Academic Press, San Diego, Calif.

Mobley, C. D., and L. Sundman (2000), *Hydrolight 4.1 Users' Guide*, 86 pp., Sequoia Scientific, Inc., Redmond, Wash.

Morel, A. (1991), Light and marine photosynthesis: A spectral model with geochemical and climatological implications, *Prog. Oceanogr.*, *26*, 263–306.

Morel, A., and A. Bricaud (1981), Theoretical results concerning light absorption in a discrete medium, and application to specific absorption of phytoplankton, *Deep-Sea Res.*, *28*, 1375–1393.

Nobileau, D., and D. Antoine (2005), Detection of blue-absorbing aerosols using near infrared and visible (ocean color) remote sensing observations, *Remote Sens. Environ.*, *95*, 368–387.

Novakov, T., V. Ramanathan, J. E. Hansen, T. W. Kirchstetter, M. Sato, J. E. Sinton, and J. A. Sathaye (2003), Large historical changes of fossil-fuel black carbon aerosols, *Geophys. Res. Lett.*, *30*(6), 1324, doi:10.1029/2002GL016345.

Patterson, E. M., D. A. Gillette, and B. H. Stockton (1977), Complex index of refraction between 300 and 700 nm for Saharan aerosols, *J. Geophys. Res.*, *82*, 3153–3160.

Pope, R. M., and E. S. Fry (1997), Absorption spectrum (380–700 nm) of pure water. II: Integrating cavity measurements, *Appl. Opt.*, *36*, 8710–8723.

Prieur, L., and S. Sathyendranath (1981), An optical classification of coastal and oceanic waters based on the specific spectral absorption curves of phytoplankton pigments, dissolved organic matter, and other particulate materials, *Limnol. Oceanogr.*, *26*, 671–689.

Prospero, J. M. (1996), The atmospheric transport of particles to the ocean, in *Particle Flux in the Ocean*, edited by V. Ittekkot et al., pp. 19–52, John Wiley & Sons, Chichester, U. K.

Ramanathan, V., P. J. Crutzen, J. T. Kiehl, and D. Rosenfeld (2001), Aerosols, climate, and the hydrological cycle, *Science*, *294*, 2119–2124.

Raphael, M. N. (2003), The Santa Ana winds of California, *Earth Interact.*, *7*, 1–13.

Rea, D. K. (1994), The paleoclimatic record provided by eolian deposition in the deep sea: The geologic history of wind, *Rev. Geophys.*, *32*, 59–196.

Rosen, H., A. D. A. Hansen, L. Gundel, and T. Novakov (1978), Identification of the graphitic carbon component of source and ambient particulates by Raman spectroscopy and an optical attenuation technique, *Appl. Opt.*, *17*, 3859–3862.

Röttgers, R., W. Schönfeld, P.-R. Kipp, and R. Doerffer (2005), Practical test of a point-source integrating cavity absorption meter: The performance of different collector assemblies, *Appl. Opt.*, *44*, 5549–5560.

Sato, M., J. Hansen, D. Koch, A. Lacis, R. Ruedy, O. Dubovik, B. Holben, M. Chin, and T. Novakov (2003), Global atmospheric black carbon inferred from AERONET, *Proc. Natl. Acad. Sci. U. S. A.*, *100*, 6319–6324.

Schuster, G. L., O. Dubovik, B. N. Holben, and E. E. Clothiaux (2005), Inferring black carbon content and specific absorption from Aerosol Robotic Network (AERONET) aerosol retrievals, *J. Geophys. Res.*, *110*, D10S17, doi:10.1029/2004JD004548.

Shinn, E. A., J. M. Smith, G. W. Prospero, P. Betzer, M. L. Hayes, V. Garrison, and R. T. Barber (2000), African dust and the demise of Caribbean coral reefs, *Geophys. Res. Lett.*, *27*, 3029–3032.

Smith, R. C., and K. S. Baker (1981), Optical properties of the clearest natural waters (200–800 nm), *Appl. Opt.*, *20*, 177–184.

Sogandares, F. M., and E. S. Fry (1997), Absorption spectrum (340–640 nm) of pure water. I. Photothermal measurements, *Appl. Opt.*, *36*, 8699–8709.

Sokolik, I. N., and O. B. Toon (1999), Incorporation of mineralogical composition into models of the radiative properties of mineral aerosol from UV to IR wavelengths, *J. Geophys. Res.*, *104*, 9423–9444.

Sokolik, I., A. Andronova, and T. C. Johnson (1993), Complex refractive index of atmospheric dust aerosols, *Atmos. Environ.*, *27A*, 2495–2502.

Solomon, P. A., T. Fall, L. Salmon, G. R. Cass, H. A. Gray, and A. Davidson (1989), Chemical characteristics of PM_10 aerosols collected in the Los Angeles area, *J. Air Pollut. Control Assoc.*, *39*, 154–163.

Sommers, W. T. (1978), LFM forecast variables related to Santa Ana wind occurrences, *Mon. Weather Rev.*, *106*, 1307–1316.

Stramski, D., and A. Morel (1990), Optical properties of photosynthetic picoplankton in different physiological states as affected by growth irradiance, *Deep-Sea Res.*, *37*, 245–266.

Stramski, D., and J. Piskozub (2003), Estimation of scattering error in spectrophotometric measurements of light absorption by aquatic particles from three-dimensional radiative transfer simulations, *Appl. Opt.*, *42*, 3634–3646.

Stramski, D., A. Bricaud, and A. Morel (2001), Modeling the inherent optical properties of the ocean based on the detailed composition of the planktonic community, *Appl. Opt.*, *40*, 2929–2945.

Stramski, D., E. Boss, D. Bogucki, and K. J. Voss (2004a), The role of seawater constituents in light backscattering in the ocean, *Prog. Oceanogr.*, *61*, 27–56.

Stramski, D., S. B. Woźniak, and P. J. Flatau (2004b), Optical properties of Asian mineral dust suspended in seawater, *Limnol. Oceanogr.*, *49*, 749–755.

Stramski, D., M. Babin, and S. B. Woźniak (2007), Variations in the optical properties of terrigenous mineral-rich particulate matter suspended in seawater, *Limnol. Oceanogr.*, *52*, 2418–2433.

Tassan, S., and G. M. Ferrari (2003), Variability of light absorption by aquatic particles in the near-infrared spectral region, *Appl. Opt.*, *42*, 4802–4810.

Twardowski, M. S., E. Boss, J. B. Macdonald, W. S. Pegau, A. H. Barnard, and J. R. V. Zaneveld (2001), A model for estimating bulk refractive index from the optical backscattering ratio and the implications for understanding particle composition in case I and case II waters, *J. Geophys. Res.*, *106*, 14,129–14,142.

Woźniak, S. B., and D. Stramski (2004), Modeling the optical properties of mineral particles suspended in seawater and their influence on ocean reflectance and chlorophyll estimation from remote sensing algorithms, *Appl. Opt.*, *43*, 3489–3503.

Yasa, Z., N. M. Amer, H. Rosen, D. A. Hansen, and T. Novakov (1979), Photoacoustic investigation of urban aerosol particles, *Appl. Opt.*, *18*, 2528–2530.

Zaneveld, J. R. V., J. Kitchen, and C. Moore (1994), The scattering error correction of reflecting-tube absorption meters, in *Ocean Optics XII*, *Proc. SPIE*, vol. 2258, edited by J. S. Jaffe, pp. 44–55, SPIE, Bellingham, Wash.

M. Cichocka, A. Cieplak, and D. Stramski, Marine Physical Laboratory, Scripps Institution of Oceanography, University of California at San Diego, 9500 Gilman Dr., La Jolla, CA 92093-0238, USA. (dstramski@ucsd.edu)

M. Stramska, Center for Hydro-Optics and Remote Sensing, San Diego State University, 6505 Alvarado Road, Suite 206, San Diego, CA 92120, USA.

S. B. Woźniak, Institute of Oceanology, Polish Academy of Sciences, Powstanców Warszawy 55, 81-712 Sopot, Poland.